



Investigation of the influence of the dimensionless centrifugal work number on spanwise rotating channel low-speed compressible flow

Junxin Che ^{1,2}, Ruquan You ^{1,2,*}, Fei Zeng,³ Haiwang Li,^{1,2} Wenbin Chen,³ and Zhi Tao^{1,2}

¹National Key Laboratory of Science and Technology on Aero Engines Aero-thermodynamics, Beihang University, Beijing 100191, China

²Research Institute of Aero-Engine, Beihang University, Beijing 100191, China

³Hunan Key Laboratory of Turbomachinery on Small and Medium Aero-Engine, Jianguo, Zhuzhou 412002, China



(Received 30 May 2023; accepted 30 October 2023; published 6 December 2023)

In the study of rotating channel flow, the key dimensionless parameters typically include the Reynolds number, rotation number, Prandtl number, and buoyancy number. Our research focused on comparing the flow characteristics between the enlarged model, analyzed under the rotating similarity theory, and the original channel flow. Significantly different flow behaviors were observed between these two cases. Through theoretical derivation and dimensional analysis, we identified a new significant parameter—the centrifugal work number. This parameter characterizes the ratio of centrifugal work to gas enthalpy in the rotating channel and plays a crucial role in measuring the compressibility of fluids within the rotating channel. Additionally, we utilized large-eddy simulation to validate the impact of the centrifugal work ratio on the flow state of the rotating channel, thus enhancing the similarity theory of rotating channel compressible flow.

DOI: [10.1103/PhysRevFluids.8.L121401](https://doi.org/10.1103/PhysRevFluids.8.L121401)

Introduction. In this paper, we introduce a dimensionless parameter, termed the centrifugal work number, derived from the rotational energy equation. This parameter quantifies the ratio of centrifugal force work to gas enthalpy in the flow within rotating channels. Large-eddy simulation (LES) was employed to validate the influence of this parameter on rotating channel flow.

In the early 1950s, the need to cool turbine blades in aviation engines pushed for research on the flow inside rotating channel since the turbine inlet temperatures were nearing the limits of the blade materials.

The introduction of similarity theory and dimensionless parameters in the study of fluid flow aims to describe and analyze the characteristics of fluid motion more effectively. For rotating channel flow, the four key dimensionless parameters typically considered are the Reynolds number, rotation number, Prandtl number, and buoyancy number. We generally use inlet parameters as global parameters for similarity studies. When the walls of the rotating channel are adiabatic, we only need to consider two parameters: the Reynolds number and the rotation number:

$$Re_{in} = \frac{\rho U_{in} D_h}{\mu}, \quad (1)$$

$$Ro_{in} = \frac{\Omega D_h}{U_{in}}, \quad (2)$$

*youruquan10353@buaa.edu.cn

where ρ is the fluid density, U_{in} is the bulk-averaged velocity at the inlet position, D_h is the hydraulic diameter of the channel, μ is the dynamic viscosity of the fluid, and Ω is the rotational speed of the channel.

By ensuring consistency among these key dimensionless parameters, the influence of rotational forces on the flow within the channel can be appropriately accounted for.

Research on the effect of centrifugal force on the flow inside rotating channels is relatively scarce. In flow with constant density, centrifugal force does not have an independent effect on the flow because its effect is generally manifested as an enhanced radial pressure, which can be combined with the pressure term to represent effective pressure:

$$p_{\text{eff}} = p - \frac{1}{2}\rho\omega^2 r^2. \quad (3)$$

However, centrifugal force may have an impact on the rotating channel flow when density changes exist in the system (Johnston, 1998) [1].

The Coriolis force plays an important role in the flow inside rotating channels, and its relative magnitude is represented by the rotational number. Barua [2] first introduced the rotational added-force term in the control equation describing the flow in spanwise rotating channels, and predicted the flow pattern of Coriolis force-induced secondary flow. Moon [3] experimentally measured the velocity profiles distribution in the core region of a straight channel under rotational conditions, and observed an increase in boundary-layer thickness near the leading side, and a decrease in boundary-layer thickness near the trailing side. Kristoffersen [4] studied the effect of Coriolis force through direct numerical simulations, while Johnston [5] investigated the effect through experiments. They all found that the mean velocity profile was pushed toward the trailing side by the Coriolis force. They also discovered that rotation stabilized the flow near the leading side but disrupted the flow near the trailing side. With the advancement of modern fluid testing techniques, Liou [6] used laser doppler velocimetry (LDV) to obtain spectral analysis of flow in rotating channels. Sante [7] and Visscher [8] observed an increase in boundary-layer thickness near the leading side and a decrease in boundary-layer velocity near the trailing side under rotational conditions using particle image velocimetry (PIV).

In recent years, research on turbulence in rotating channels has become increasingly deep. Regarding the impact of rotation on turbulence, Nakabayashi [9] and Brethouwer [10,11] found that even in high Reynolds number channels, the leading side begins to transition to laminar flow as the rotation number increases. However, at high Reynolds number and high rotation speeds, linearly unstable Tollmien-Schlichting-like waves can cause sustained bursting of turbulence. Grundestam [12] discovered that a balance between negative turbulence production mechanisms played a significant role in maintaining the relatively distinct interface between the two regions.

Experimental studies of the flow and heat-transfer characteristics in rotating machinery internal cooling channel are limited by experimental conditions and testing techniques, requiring the scaling up of research models. Through dimensional analysis of the energy equation, we obtained another critical dimensionless parameter that determines the compressibility of the flow in the rotating channel and verified the effects of this dimensionless parameter.

Derivation of rotational dimensionless parameters. In a rotating channel, the energy equation that neglects radiation heat transfer is shown in expression (4):

$$\nabla \left[\left(\rho e + \rho \frac{V^2}{2} + p \right) \vec{V} \right] = \nabla(\lambda \nabla T) - \rho \vec{\Omega} \times (\vec{\Omega} \times \vec{r}) \cdot \vec{V} + \nabla \cdot (\vec{V} \cdot \tau_{ij}), \quad (4)$$

where ∇ is the Hamiltonian operator, ρ is the density, e is the internal energy of the fluid, \vec{V} is the velocity vector, p denotes the pressure, λ represents the thermal conductivity of the fluid, T represents the temperature, Ω represents rotation speed of the channel, and τ_{ij} denotes the tensor form of viscous force. In rotating channels, the impact of viscous forces on energy compared to positive pressure is much smaller, so the energy equation for steady flow neglecting the work done

by viscous forces can be expressed as expression (5):

$$\nabla \left[\left(\rho e + \rho \frac{V^2}{2} + p \right) \vec{V} \right] = \nabla(\lambda \nabla T) - \rho \vec{\Omega} \times (\vec{\Omega} \times \vec{r}) \cdot \vec{V}. \quad (5)$$

Simplifying and expressing the relative magnitude of total energy in terms of enthalpy and kinetic energy, there are only two ways to change the total energy of fluids in a rotating channel: heat transfer and work done by centrifugal force:

$$\nabla \left[\rho c_p T \vec{V} + \rho \frac{V^2}{2} \vec{V} \right] = \nabla(\lambda \nabla T) - \rho \vec{\Omega} \times (\vec{\Omega} \times \vec{r}) \cdot \vec{V}. \quad (6)$$

The change in energy in a rotating channel is mainly achieved through heat transfer and work done by centrifugal force. To examine the similarity of flow, different flow fields need to be compared, and the various terms in the energy equation need to be made dimensionless. Let c_{p0} , U_0 , ρ_0 , θ_0 , D_0 , and r_0 represent the characteristic physical quantities of specific heat at constant pressure, velocity, density, temperature, length, and rotation radius, respectively:

$$c_p^* = \frac{c_p}{c_{p0}}, \quad \vec{V}^* = \frac{\vec{V}}{U_0}, \quad \rho^* = \frac{\rho}{\rho_0}, \quad T^* = \frac{T}{\theta_0}, \quad \vec{r}^* = \frac{\vec{r}}{r_0}. \quad (7)$$

By substituting dimensionless quantities into the energy equation, expression (8) is obtained:

$$\begin{aligned} & \left(\frac{\rho_0 c_{p0} T_0 U_0}{D_0} \right) \nabla^* (\rho^* c_p^* \theta^* \vec{V}^*) + \left(\frac{\rho_0 U_0^3}{D_0} \right) \nabla^* \left(\rho^* \frac{V^{*2}}{2} \vec{V}^* \right) \\ & = \left(\frac{\lambda T_0}{D_0^2} \right) \nabla^* (\nabla^* \theta^*) - (\rho_0 \Omega^2 r U_0) \rho^* [\vec{i} \times (\vec{i} \times \vec{r}^*)] \cdot \vec{V}^*. \end{aligned} \quad (8)$$

The dimensionless energy equation can be simplified and expressed as expression (9) after rearrangement:

$$\begin{aligned} & \nabla^* (\rho^* c_p^* \theta^* \vec{V}^*) + \left(\frac{U_0^2}{c_{p0} T_0} \right) \nabla^* \left(\rho^* \frac{V^{*2}}{2} \vec{V}^* \right) \\ & = \left(\frac{\lambda}{\rho_0 U_0 D_0 c_{p0}} \right) \nabla^* (\nabla^* \theta^*) - \left(\frac{\Omega^2 r_0 D_0}{c_{p0} T_0} \right) \rho^* [\vec{i} \times (\vec{i} \times \vec{r}^*)] \cdot \vec{V}^*. \end{aligned} \quad (9)$$

From the above dimensionless energy equation, it is clear that as long as the corresponding dimensionless combinations of parameters for the two flow phenomena are the same, then they are similar. These dimensionless combination coefficients are the control criteria for flow similarity.

$\frac{\Omega^2 r_0 D_0}{c_{p0} T_0}$ represents the ratio of the work done by centrifugal force to the enthalpy of the fluid, which characterizes the relative magnitude of work done by centrifugal force. The dimensionless parameters can be expressed in terms of commonly used parameters, which can be simplified as follows:

$$\frac{\Omega^2 r_0 D_0}{c_{p0} T_0} = \frac{\frac{D_0}{r_0}}{\frac{c_{p0} T_0}{\Omega^2 r_0^2}} = \frac{\frac{D_0}{r_0}}{\frac{1}{(k-1)U_\Omega^2}} = (k-1) Ma_\Omega^2 \frac{D_0}{r_0}, \quad (10)$$

where Ma_Ω is the rotating Mach number:

$$Ma_\Omega^2 = \frac{U_\Omega^2}{\sqrt{k R_g T}} = \frac{\Omega^2 r_0^2}{\sqrt{k R_g T}}, \quad (11)$$

where U_Ω is the rotational linear velocity. R_g is a gas constant and its value is 287.06 J/(kg K).

The rotational linear speed U_Ω of the channel is a crucial variable that determines the compressibility effects of the fluid. It can be understood that higher rotational linear speed results in

more significant centrifugal compression effects. Therefore, the rotating Mach number Ma_Ω directly represents the key parameter for indicating the rotational compressibility effects.

Although a dimensionless parameter has been obtained in the energy equation, further verification is still needed to determine the magnitude of its impact on the flow.

Discussion. In order to simplify the expression, we will refer to the parameter that characterizes the impact of the work done by centrifugal force on the flow as the centrifugal work number, denoted as CW :

$$CW = Ma_\Omega^2 \frac{D_h}{r}. \quad (12)$$

Here, we simplify the flow in the rotating channel into a one-dimensional radial flow, and then derive the effect of centrifugal work on fluid compressibility.

The one-dimensional momentum equation in the z direction of the channel, neglecting frictional forces, can be expressed as

$$w \frac{dw}{dz} = \Omega^2 r - \frac{1}{\rho} \frac{dp}{dz}. \quad (13)$$

The speed of sound of the idea gas can be expressed as

$$c^2 = \frac{dp}{d\rho}. \quad (14)$$

By substituting the momentum equation (13), we obtain

$$w^2 \frac{dw}{w} = \Omega^2 r dz - \frac{d\rho}{\rho} c^2, \quad Ma^2 \frac{dw}{w} = \frac{\Omega^2 r dz}{c^2} - \frac{d\rho}{\rho}, \quad \frac{d\rho}{\rho} = CW \frac{dz}{D_h} - Ma^2 \frac{dw}{w}. \quad (15)$$

It can be seen that the change in fluid density is mainly affected by the CW and Ma . In order to further explore the effect of the CW on the compressibility of the fluid, let us simplify the equation further:

$$\frac{d\rho}{\rho} = CW \frac{dz}{D_h} - Ma^2 \frac{d\left(\frac{\dot{m}}{\rho A}\right)}{\frac{\dot{m}}{\rho A}}. \quad (16)$$

Assuming there is no flow out and the cross-sectional area remains constant along the duct, we can further simplify the equation:

$$\frac{d\rho}{\rho} = CW \frac{dz}{D_h} + Ma^2 \frac{d\rho}{\rho}, \quad (17)$$

$$\frac{d\rho/\rho}{dz/D_h} = \frac{CW}{1 - Ma^2}. \quad (18)$$

The rate of change of density per unit length is influenced by both Ma and the centrifugal work number (CW).

When the Mach number of the flow inside the rotating channel is less than 0.3, the effect of fluid density variation rate is about 0.1 times that of the CW . We define the compressible flow inside the rotating channel as a low-speed compressible flow. The equation can be simplified as follows:

$$\frac{d\rho/\rho}{dz/D_h} = CW. \quad (19)$$

Therefore, in the low Mach number flow inside the rotating channel, the key factor determining the compressibility of the fluid is the CW . In engineering applications research, we need to pay special attention to the impact of compressibility effects generated by centrifugal force on the flow in rotating channels. Conclusions that do not consider compressibility effects and simply investigate the effects of Coriolis force, buoyancy force, and other effects may not reflect the real flow state.

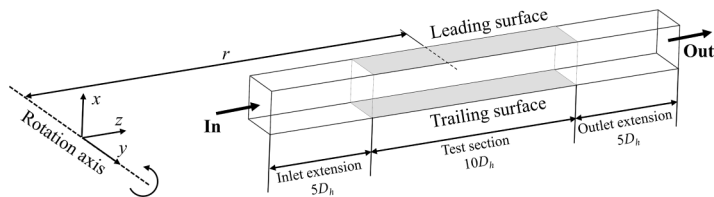


FIG. 1. Sketch of physical configuration and computational model.

The influence of CW on rotating channel flow.

A. *Test section and numerical methods.* The test section is shown in Fig. 1. The section of the model is a rectangular shape with an aspect ratio of 1. The length of the test section is $10D_h$, and $5D_h$ of extended sections are set at the inlet and outlet to eliminate the influence of the inlet and outlet boundary on the flow in the test section.

In order to accurately predict the flow inside the rotating channel, large-eddy simulation is adopted. The code utilized was FLUENT. Nonuniform grids are used to partition the cross sections perpendicular to the flow direction. Grid refinement is applied near the walls, with a grid spacing of approximately $y^+ \approx 0.5$ for the first layer near the wall. Additionally, the maximum grid spacing in the mainstream region is approximately $\Delta y^+ \approx 20$ and $\Delta x^+ \approx 20$. The z direction of the model is divided using a uniform grid with $\Delta z^+ \approx 40$. The computational domain is divided into $200 \times 200 \times 1500$ elements. The WALE model was chosen for the subgrid-scale modeling in LES.

As shown in Fig. 2, this study compares the mainstream mean velocity profiles obtained using LES with the ones computed by Kristoffersen [4] using direct numerical simulation (DNS) for a rotating channel. The maximum error in the mainstream velocity profiles obtained through LES is less than 2%. Therefore, it can be concluded that the numerical methods employed in our study can effectively predict the mainstream velocity profiles inside the rotating channel.

B. *Mean flow characteristics with different CW.* In a rotating adiabatic channel, modeling the flow only requires maintaining geometric and aerodynamic similarity, without considering the influence of centrifugal force. To achieve this, a consistent aspect ratio ($r/D_h = 70$), and the same aerodynamic parameters, such as Reynolds number ($Re = 50000$) and rotation number ($Ro = 0.412$), can be used. Based on this, the original model was scaled up. The parameter values for various models are presented in Table I.

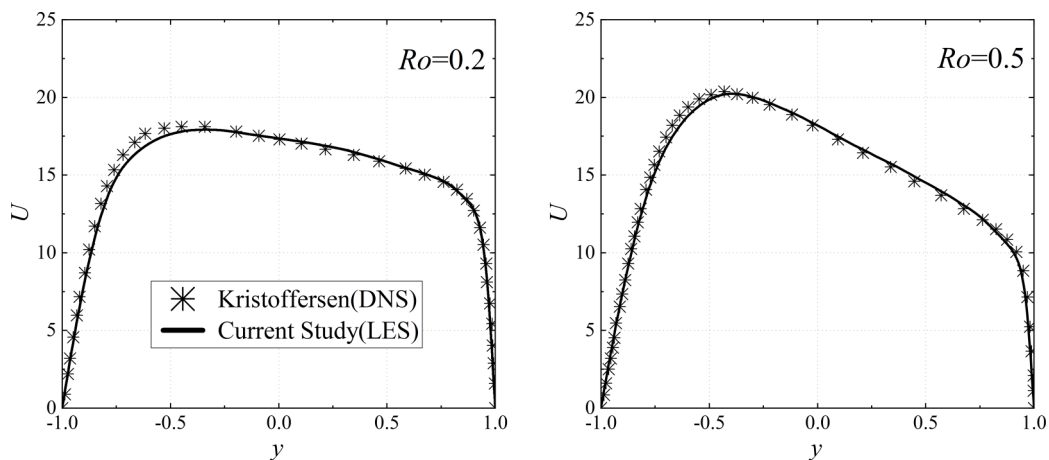


FIG. 2. Comparison of mainstream velocity profiles between LES and DNS.

TABLE I. Model parameters validating the influence of CW

D_h/mm	5	6	10	20
T_{in}/K	773			
p_{in}/Pa	2×10^6			
n/rpm	16000	11111	4000	1000
Ma	3.65×10^{-2}	2.97×10^{-2}	1.78×10^{-2}	8.91×10^{-3}
Ma_{Ω}	1.11	0.769	0.277	0.069
CW	1.58×10^{-2}	1.10×10^{-2}	3.95×10^{-3}	9.88×10^{-4}

The density and temperature variations within the channel are shown in Fig. 3. In a channel with a length of $20D_h$, the outlet density increases by 34.1% and the temperature increases by 13.0% compared to the inlet. This means that the flow in the channel of rotating machines cannot be treated simply as incompressible flow.

We also verified the relationship between the density variation and the centrifugal work CW [Eq. (19)]. The CW provides a good prediction accuracy for the density variation within a certain length range. Taking the 5-mm channel as an example, the maximum prediction error occurs at the outlet position, but it is still less than 2%.

The velocity distribution of the cross section along the channel of each hydraulic diameter is shown in Fig. 4, under the condition of the same inlet temperature (T_{in}) and inlet pressure (P_{in}). The mean velocity distribution of the cross section along the channel of different hydraulic diameter models is shown in Fig. 4.

Although the same dimensionless parameters were maintained during the model-scaling process, there were significant differences in the flow fields of the channel. In the small-scale model, the boundary layer near the leading side develops rapidly along the channel. As the fluid near the leading side decelerates, flow separation even occurs near the leading side in small-sized channels ($D_h = 5$ and 6 mm). See Fig. 5.

We know that the choice of outlet boundary conditions is crucial in LES as it may have a significant impact on flow separation near the leading side. To validate if the separation region is influenced by the outlet boundary, we extended the outlet by an additional $10D_h$ while keeping the inflow parameters identical to the original model. Extending the channel did not have any influence on the flow at the investigated positions, and the location of the separation region remained almost

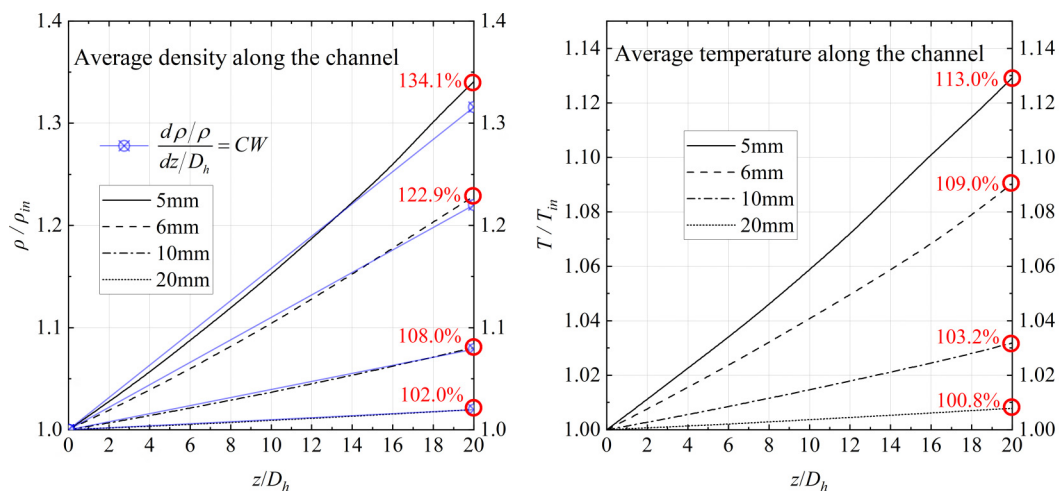


FIG. 3. Distribution of average density and temperature along the channel for different hydraulic diameters.

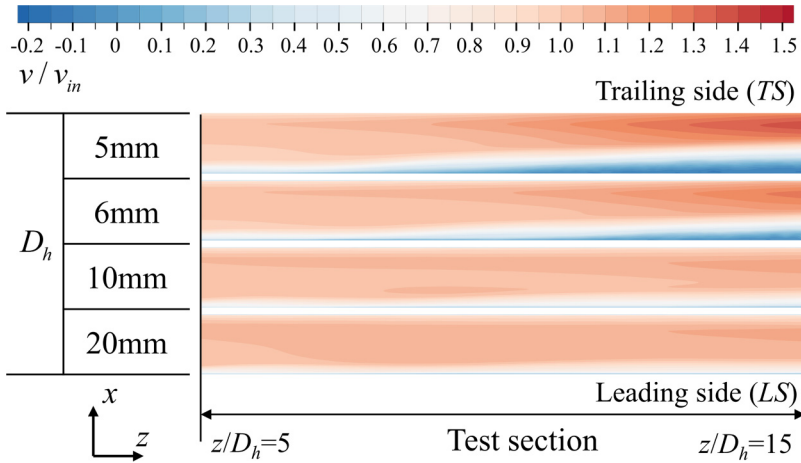


FIG. 4. Comparison of cross-sectional dimensionless mean velocity distribution in similarity models with different hydraulic diameters.

unchanged (Figs. 6 and 7). This indicates that the observed flow separation near the leading side is physically real and is not affected by the outlet conditions.

The flow separation near the leading side implies that the effect of centrifugal work on the fluid is not simply a result of compressing the fluid. Indeed, during the compression process, there must exist a radial force that causes a rapid deceleration of the fluid near the leading side and can even lead to flow separation. This effect even has a greater impact on the flow than the mere compression effect itself.

However, in the large-scale similar model, even though the channel had the same inlet Re and inlet Ro , the enlarged model was unable to model the state of flow.

This also implies that the centrifugal work number is a critical parameter to consider in the process of similarity analysis. In the model of the internal cooling channel of the rotating machinery studied, the flow characteristic changes caused by centrifugal work number cannot be ignored.

C. Mean flow characteristics under the same CW. To verify the influence of CW on the similarity process of rotating channels, we conducted additional similarity studies on channels while keeping the CW constant. As shown in Table II, when transforming from model 0 to model 1 and 2, the

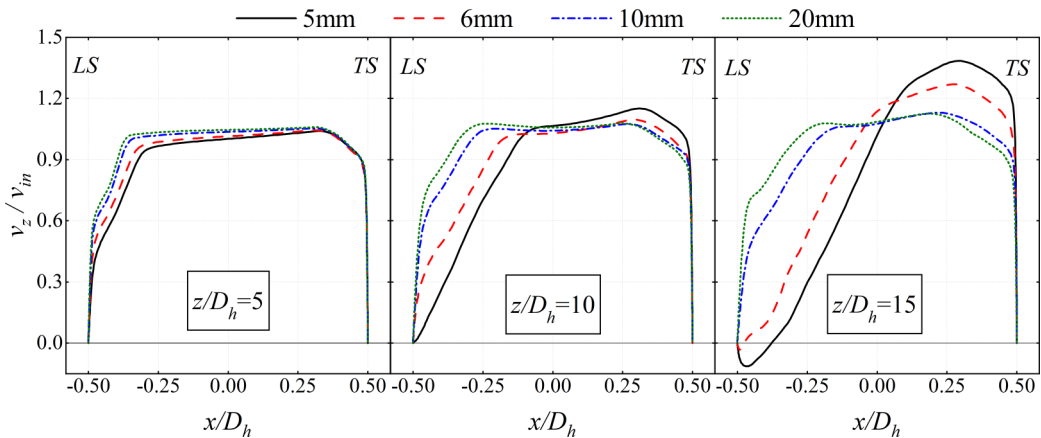


FIG. 5. Streamwise mean velocity profiles along channels of different scaling models.

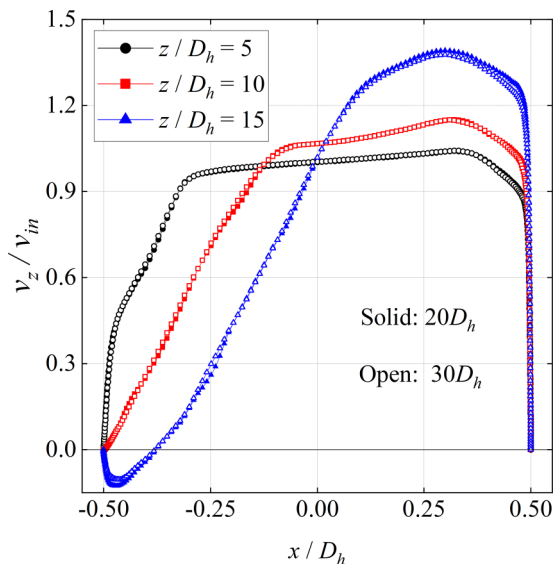


FIG. 6. Velocity profiles comparison of three flow sections in models with channel lengths of $20D_h$ and $30D_h$.

hydraulic diameter was enlarged from 5 to 20 mm, and the corresponding inlet pressure was reduced to achieve the matching of the inlet Mach number, thus obtaining a series of similarity results where the inlet Re , Ro , CW , and r/D_h all remained consistent. Models 3 and 4 considered the use of ambient-temperature gas in laboratory experiments, and the inlet temperature was changed to 300 K while still keeping the above key parameters consistent.

When keeping the CW the same, the nondimensional velocity field in the middle cross section of the channel is shown in Fig. 8. After introducing nondimensional parameters, the development status of the flow along the channel is almost identical to that of the original model. The velocity profile along the spanwise cross section remains similar to that of the original model after amplification (Fig. 9). Therefore, it can be verified that the key nondimensional parameter CW derived from the energy equation is the key nondimensional parameter that needs to be consistent in the study of rotational similarity.

Conclusion. This paper employs dimensional analysis and theoretical derivation to introduce a significant dimensionless parameter, known as the centrifugal work number (CW):

$$CW = Ma_{\Omega}^2 \frac{D_h}{r}. \quad (20)$$

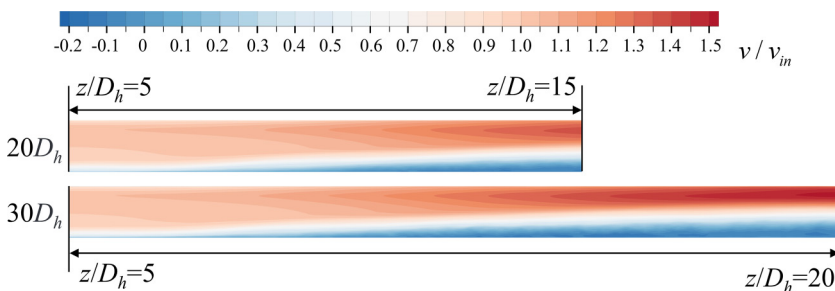


FIG. 7. Velocity profiles of the midsection ($x = 0$) in models with channel lengths of $20D_h$ and $30D_h$.

TABLE II. Model parameters for different hydraulic diameter models with the same CW .

Model	0	1	2	3	4
D_h/mm	5	10	20	10	20
T_{in}/K	773	773	773	300	300
p_{in}/Pa	2×10^6	1×10^6	5×10^5	6.23×10^5	3.15×10^5
n/rpm	16 000	8000	4000	4983	2492
Ma			3.65×10^{-2}		
Ma_Ω			1.11		
CW			1.58×10^{-2}		

The CW represents the ratio of centrifugal work to gas enthalpy and plays a crucial role in determining the compressibility of flow within rotating channels. In typical internal cooling channels of rotating machinery, the compression effect of the flow cannot be disregarded due to the substantial value of the centrifugal work number.

Consequently, the similarity rules derived from the incompressible Navier-Stokes equations (maintaining geometric similarity, as well as identical values of Re , Ro , r/D_h , and Buo) fail to adequately describe the flow state within these channels. For compressible flow in rotating channels, matching the centrifugal work number becomes an essential requirement.

Through theoretical derivation, we establish the relationship between flow compressibility and the centrifugal work number in a low-speed channel. The estimation of the density change [Eq. (21)] is verified by the numerical results.

$$\frac{d\rho/\rho}{dz/D_h} = CW. \quad (21)$$

The increase of CW not only causes the increase of the density and temperature in the channel, but also changes the mean velocity distribution of the fluid in the channel. As the CW increases, the fluid near the trailing side accelerates, and the low-speed region near the leading edge rapidly develops, even leading to flow separation. On one hand, this phenomenon is caused by the enhanced

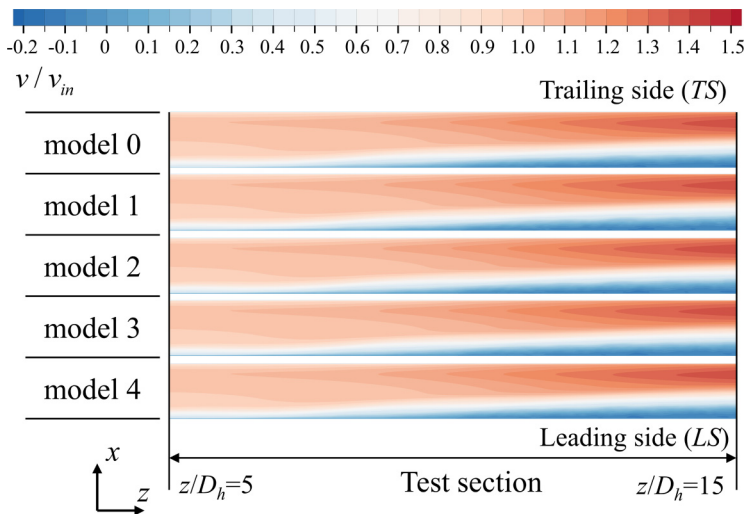


FIG. 8. Distribution of dimensionless velocity field in cross sections of similarity models with consistent inlet CW .

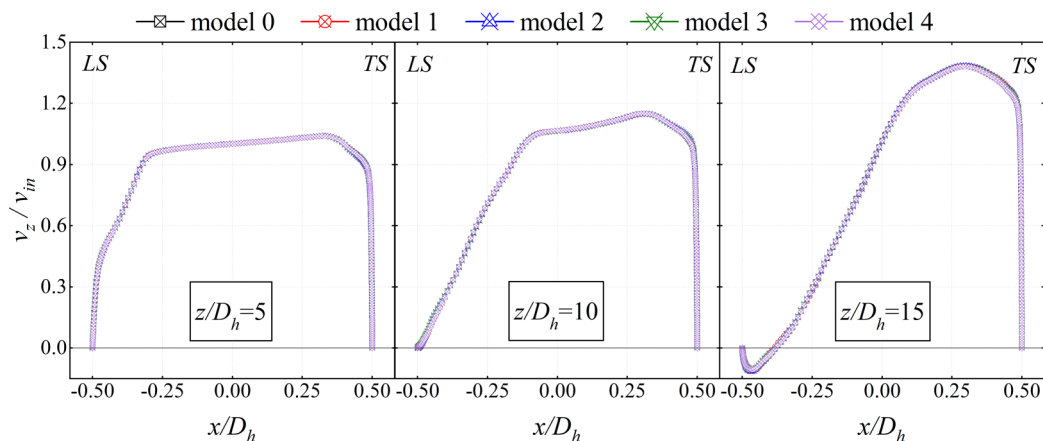


FIG. 9. Streamwise velocity profiles along channels of different scaling models with consistent inlet CW .

relative effect of the Coriolis force. On the other hand, the occurrence of flow separation indicates that the increase in centrifugal work leads to the radial forces that accelerate or decelerate the fluid at different positions within the channel.

In this study, we have observed the occurrence of flow separation within spanwise adiabatic rotating channel. Flow separation near the leading side can introduce additional complexities and challenges to the study of rotating channel flows. It highlights the importance of considering factors such as CW and flow conditions when analyzing and predicting flow behavior. This observation opens up opportunities for further investigation and understanding of the underlying physics involved in these flows.

In summary, this research provides valuable insights into the understanding of centrifugal forces in fluid dynamics and offers practical guidance for the design and optimization of flow systems within rotating channels.

Acknowledgments. This work was supported by National Science Fund for Distinguished Young Scholars (Grant No. 52225602). This work was supported by Beijing Municipal Natural Science Foundation (Grant No. 3222034). This work was sponsored by Beijing Nova Program (Grant No. 20220484129). This work was sponsored by National Science and Technology Major Project (Grant No. J2019-II-0022-0043).

The authors report no conflict of interest.

-
- [1] J. P. Johnston, Effects of system rotation on turbulence structure: A review relevant to turbomachinery flows, *Int. J. Rotating Mach.* **4**, 97 (1998).
 - [2] S. N. Barua, Secondary flow in a rotating straight pipe, *Proc. R. Soc. London, Ser. A* **227**, 133 (1954).
 - [3] I. Moon, Effect of Coriolis force on the turbulent boundary layer in rotating fluid machines, Ph.D. thesis, Gas Turbine Laboratory Rep. No. 74, Massachusetts Institute of Technology, 1964.
 - [4] R. Kristoffersen and H. I. Andersson, Direct simulations of low-Reynolds-number turbulent flow in a rotating channel, *J. Fluid Mech.* **256**, 163 (1993).
 - [5] J. P. Johnston, R. M. Halleent, and D. K. Lezius, Effects of spanwise rotation on the structure of two-dimensional fully developed turbulent channel flow, *J. Fluid Mech.* **56**, 533 (1972).
 - [6] T.-M. Liou, M.-Y. Chen, and K.-H. Chang, Spectrum analysis of fluid flow in a rotating two-pass duct with detached 90° ribs, *Exp. Therm Fluid Sci.* **27**, 313 (2003).

- [7] A. Di Sante and R. A. Van den Braembussche, Experimental study of the effects of spanwise rotation on the flow in a low aspect ratio diffuser for turbomachinery applications, *Exp. Fluids* **49**, 585 (2010).
- [8] J. Visscher and H. I. Andersson, Particle image velocimetry measurements of massively separated turbulent flows with rotation, *Phys. Fluids* **23**, 075108 (2011).
- [9] K. Nakabayashi and O. Kitoh, Turbulence characteristics of two-dimensional channel flow with system rotation, *J. Fluid Mech.* **528**, 355 (2005).
- [10] G. Brethouwer, Linear instabilities and recurring bursts of turbulence in rotating channel flow simulations, *Phys. Rev. Fluids* **1**, 054404 (2016).
- [11] G. Brethouwer, Statistics and structure of spanwise rotating turbulent channel flow at moderate Reynolds numbers, *J. Fluid Mech.* **828**, 424 (2017).
- [12] O. Grundestam, S. Wallin, and A. V. Johansson, Direct numerical simulations of rotating turbulent channel flow, *J. Fluid Mech.* **598**, 177 (2008).